Diffusive behaviors of circle-swimming motors

Nathan A. Marine, Philip M. Wheat, Jesse Ault, and Jonathan D. Posner

Diffusive Behaviors of Circle Swimming Motors

Nathan A. Marine,[1] Philip M. Wheat,[1] Jesse Ault,[2] and Jonathan D. Posner[3,4*]

[1]*Mechanical Engineering, Arizona State University, Tempe, Arizona 85287*
[2] *Department of Mechanical Engineering, Purdue, Indiana 47907*
[3]*Department of Mechanical Engineering, University of Washington, Seattle, Washington 98195*
[4]*Department of Chemical Engineering, University of Washington, Seattle, Washington 98195*

*Corresponding author.

Spherical catalytic micromotors fabricated as described in Wheat et al. 2010 show fuel concentration dependent translational and rotational velocity. The motors possess short-time and long-time diffusivities that scale with the translational and rotational velocity with respect to fuel concentration. The short-time diffusivities are 2-3 orders of magnitude larger than the diffusivity of a Brownian sphere of the same size, increase linearly with concentration, and scale as $v^2/2\omega$. The measured long-time diffusivities are 5 times lower than the short-time diffusivities, scale as $v^2/[2D_r(1+(\omega/D_r)^2)]$, and exhibit a maximum as a function of concentration. Maximums of effective diffusivity can be achieved when the rotational velocity has a higher order of dependence on the controlling parameter(s), for example fuel concentration, than the translational velocity. A maximum in diffusivity suggests that motors can be separated or concentrated using gradients in fuel concentration. The decrease of diffusivity with time suggests that motors will have a high collision probability in confined spaces and over short times; but will not disperse over relatively long distances and times. The combination of concentration dependent diffusive time scales and non-monotonic diffusivity of circle swimming motors suggests that we can expect complex particle responses in confined geometries and in spatially dependent fuel concentration gradients.

I. INTRODUCTION

Synthetic nanomotors are being developed to mimic nanoscale biomotors present in biological systems. Efforts in this area range from synthetic modifications on existing biomotors [1–5] to purely synthetic catalytic bimetallic nanomotors [6–8]. Motion of the synthetic motors has been achieved using a number of propulsion mechanisms including auto-diffusiophoresis [9–11], auto-electrophoresis [6,7,12–14], and bubble generation [15,16]. There are numerous reviews of motors and we point to Ebbens and Howse [17] for a general review of motors and to Paxton, Sen & Mallouk [7] or Wang [18] for reviews self-electrophoretic motors.

Bimetallic nanomotors have been engineered to swim at 100 body lengths per second as well as pick up, haul, and release micrometer-scale cargo [19,20]. Their motion can be controlled using external magnetic fields [19,21] as well as chemical [22–24] and thermal [25] fields.

Catalytic bimetallic nanomotors propel themselves by electrocatalytically decomposing hydrogen peroxide (H_2O_2) [7,14,26,27] through a mechanism we recently described as reaction induced charge auto-electrophoresis (RICA) [26,27]. Bimetallic nanomotors in an aqueous hydrogen peroxide solution catalyze peroxide oxidation at one of the metal surfaces (anode), generating protons, electrons, and oxygen molecules. The electrons conduct through the motor to the other metal surface (cathode) and complete the reduction reaction by combining with protons, peroxide, and oxygen to generate water. The asymmetric reactions result in an excess and depletion of protons in the surrounding electrolyte at the anode and cathode ends, respectively. The proton imbalance results in asymmetric free charge density, which generates an electric dipole and field pointing from the anode to the cathode. In addition, the particle's negative surface charge attracts cations from the bulk solution which form a positively charged diffuse screening layer surrounding the particle. The self-generated electric field couples with the charge density induced by both the reactions and the diffuse layer to produce an electrical body force that drives fluid from the anode to the cathode. The fluid motion results in locomotion of the motor in the direction of the anode. Net motion of the nanomotor requires some native charge, or zeta potential. The nanomotor velocity is linearly dependent on the reaction flux density and the native surface charge [26,27]. Most synthetic motors are rotationally diffusive, which means that although the motors have an advective velocity controlled mainly by some chemical concentration, their orientation is dictated by Brownian fluctuations.

Motors that are fabricated to swim with nonzero mean rotational velocity, ω, in addition to rotational Brownian motion, are capable of more complex motion than rotationally diffusive swimmers. We classify motors with nonzero mean translational and rotational velocities as circle swimmers. Circle swimming motors can be fabricated by combining two individual motors [10] or by growing an additional segment [28,29] on the motor such that an asymmetric force profile is generated. Ebbens et al. studied the behavior of these diffusiophoretic Janus doublet particles and noted that the radius of curvature of the circle swimming doublets depends on the respective orientations of the particles within the doublet [10].

In this work, we study the diffusivity of $3\,\mu m$ spherical catalytic bimetallic circle swimmers over short and long time scales as a function of hydrogen peroxide concentration. We fabricate the motors using multistep metal deposition process on polystyrene microspheres that we reported earlier [30]. We compare the behavior of these motors to Brownian dynamics simulations, simple analytical theory, and to previously published work by Ebbens et al. [10]. The motors exhibit both translational and mean rotational velocities that depend on H_2O_2 concentration. We show that generic circle swimmer motors (not necessarily catalytic motors) exhibit short-time and long-time diffusivities that scale as $v^2/2\omega$ and $v^2/[2D_r(1+(\omega/D_r)^2)]$ respectively. The experimental long-time diffusivities exhibit a maximum diffusivity as a function of concentration because the translational and angular velocities deviate from the linear trend as shown in Figure 2. The deviations are not systematic (i.e. not because the velocity as a function of concentration exhibit some significant nonlinearity). The deviation from the fit is due to natural variation of the swimmer's velocity. We expect that with a larger sample

volume or more uniform motors, we may not observe the asystematic variation in velocity that yields the maximum in effective diffusivity, however we provide some simple examples of the conditions under which maximums in effective diffusivities may be observed. Generally, we find that a maximum in long-time effective diffusivity can be achieved in a system where either v and ω exhibit some nonlinear dependence on concentration (or any other driving potential). Another method by which a maximum in in diffusivity could be achieved is through the modulation of the rotational diffusivity. It is possible to modulate the rotational diffusivity through an unsteady swimming mechanism, as we show in work, or through the curvature of a swimming rod as is shown in Takagi et al. 2013 [31].

II. THEORY

The time-averaged displacement of particles with an advective component, such as swimming organisms and the motors described here, can be described by their effective diffusivity. The effective diffusivity combines the effects of rotational diffusion, translational diffusion, and advective motion of the motors. Experimentally, the effective diffusivity can be determined by assembling the mean squared displacement (MSD) of a set of particles and finding the slope. The MSD is determined by taking the ensemble average (to minimize errors due to variability between particles and of individual particles in time) of the squared displacement (SD) of individual particles. The shape of the MSD determines what region the slope is taken for the diffusivity. The MSD is always initially quadratic since the particle must initially move directly away from its origin. Typically the quadratic region transitions into a linear long-time region where the classical diffusivity is the slope divided by 2^n, where n is the number of dimensions over which the displacement is tracked.

The long-time behavior of rotationally diffusive motors was studied by Howse et al. for platinum Janus particles that swim by auto-diffusiophoresis in hydrogen peroxide [9]. By calculating the MSD of the motors they were able to determine the effective diffusivity of the motors as a function of concentration and show that for rotationally diffusive swimmers the long-time effective diffusivity is [9]

$$D_L = D_o + \frac{v^2}{4D_r}$$

(1)

where D_o is the Brownian translational diffusivity, v is the velocity of the motor, and D_r is the Brownian rotational diffusivity. From Stokes-Einstein, the Brownian translational diffusivity of a sphere is $D_o=k_BT/6\pi\mu a$ and the Brownian rotational diffusivity is $D_r=k_BT/8\pi\mu a^3$, where k_BT is the thermal energy, μ is the dynamic viscosity of water, and a is the radius of the sphere [35]. This means that rotationally diffusive swimmers, like catalytic bimetallic nanorods, with considerable advective velocities are capable of achieving effective diffusivities approximately 4 orders of magnitude larger than that of a Brownian particle of the same size [32].

For circle swimmers the shape of the MSD can be determined by solving the appropriate Langevin equations. The standard Langevin equations are reduced to 2-D because the motors settle near the surface and are modified such that the displacement of the motors is the sum of its advective and Brownian components as shown in Equations 2-4 [10,33].

$$\frac{dx(t)}{dt} = v\cos\theta(t) + \xi_1(t) \tag{2}$$

$$\frac{dy(t)}{dt} = v\sin\theta(t) + \xi_2(t) \tag{3}$$

$$\frac{d\theta(t)}{dt} = \omega + \zeta(t) \tag{4}$$

Where ω is the rotational velocity, x and y are the location of the center of mass, and θ is the orientation of the motors. The Brownian fluctuations terms, ξ and ζ, are Gaussian random variables with zero mean and whose magnitudes are determined from theoretical isotropic Brownian diffusivities. In Ebbens et al. 2010 and van Teeffelen and Löwen 2008 Equations 2-4 are solved to determine the MSD,

$$\Delta L^2(t) = 4Dt + \frac{2v^2 D_r t}{D_r^2 + \omega^2} + \frac{2v^2(\omega^2 - D_r^2)}{(D_r^2 + \omega^2)^2}$$
$$+ \frac{2v^2 e^{-D_r t}}{(D_r^2 + \omega^2)^2}\left[(D_r^2 - \omega^2)\cos\omega t - 2\omega D_r \sin\omega t\right] \tag{5}$$

The MSD switches from a sinusoidal short-time region to a long-time region when $t > \pi/\omega$. We term the sinusoidal region the short-time region and we define the short-time diffusivity, D_S, from the slope of the linear region of the first rising wave. Everything that follows the first rising wave is considered the long-time region with a long-time diffusivity, D_L. As is shown in Ebbens et al. 2010, Equation 5 can be used to solve for the long-time diffusivity of a circle swimmer [10],

$$D_L = D_o + \frac{v^2}{2D_r\left[1 + \left(\dfrac{\omega}{D_r}\right)^2\right]} \tag{6}$$

Equation 6 shows that the rotational thermal motion modulates the effective long-time diffusivity through the translational and angular velocities. The translational thermal motion, D_o, on the other hand is only additive. A circle swimmer with no rotational Brownian motion swims in a perfect circle with an origin that drifts with D_o and thus will have a long-time effective diffusivity equal to the Brownian translational diffusivity. For a detailed discussion of the

interaction between the advective motion and Brownian motion see the Supplemental Material (SM1-3) and for a detailed discussion of variable rotational diffusivity see Figure 7b.

In order to find the short-time diffusivity we solve Equations 2-4 assuming that the rotational diffusivity is small compared to the rotational velocity over short times, given as,

$$D_S = D_o + \frac{v^2}{2\omega}. \tag{7}$$

This equation is similar to what we observe for the long-time behavior of rotationally diffusive swimmers (Equation 1) except that the rotational diffusivity is replaced by the rotational velocity. Equation 7 is also similar to Equation 6 except that it scales as v^2/ω instead of v^2/ω^2 because we assumed the rotational diffusivity to be small in the short-time region. Equation **7** is applicable when the motor has completed less than one half of a rotation or $t<\pi/\omega$. For the range of rotational velocities in this paper the short-time region ranges from 2 s to 120 s.

For particles where the translational and rotational velocities both depend on a third parameter, here fuel concentration, we can rewrite the velocities in terms of that parameter,

$$v(C) = AC^a \tag{8a}$$

$$\omega(C) = BC^b \tag{8b}$$

where C is concentration, A (μm/s/M^a), B (rad/s/M^b), and a, b are constants. In this case the short-time diffusivity and long-time diffusivity scale as,

$$D_S \propto C^{2a-b} \tag{9a}$$

$$D_L \propto \frac{C^{2a}}{1+C^{2b}}. \tag{9b}$$

Equation 9 predicts that if both the translational and rotational velocities depends linearly on fuel concentration then the short-time diffusivity scales linearly with fuel concentration while the long-time diffusivity increases with concentration and then asymptotes at higher concentrations.

III. EXPERIMENTAL METHODOLOGY

We fabricate 3μm bimetallic gold and platinum spherical micromotors using a multistep metal deposition process on polystyrene microspheres that we reported earlier [30]. In brief, a 1% volume fraction aqueous dispersion of 3 μm fluorescent polystyrene spheres ($\rho = 1.05$ g/cm^3,

Duke Scientific Inc, Fremont, CA, USA) are deposited onto a 2.5 x 2.5 cm^2 square glass substrate. The solvent evaporates at room temperature, forming a monolayer of spheres. The upper hemispheres are coated with 20 nm of gold using a sputter coater (Cressington 108 auto, Cressington Scientific Instruments, Watford WD19 4BX, England, UK). The half-coated spheres are re-suspended in an aqueous solution and then deposited in random orientations into a monolayer on a clean glass slide. This process is repeated until the spheres are fully coated. The fully Au coated spheres are re-deposited on a clean substrate and coated with 20 nm platinum resulting in a Janus sphere that is half coated with gold and half platinum.

Transmission optical microscopy is used to observe the swimming nanomotors. We use an inverted microscope (Nikon TE2000, Japan) with a 20x objective (NA=0.6) and 100 W halogen illumination (Nikon TE2 PS 100W, Japan). The images are captured using a cooled CCD camera (Cascade IIb, Photometrics, Tucson, AZ). Hydrogen peroxide (Sigma-Aldrich, St. Louis, MO) is used at concentrations of 0.063%, 0.135%, 0.253%, 0.5%, 0.75%, 1.0%, and 1.25% (vol). Experiments are performed in chambered glass wells with an area of 0.4 cm^2 (cat. no. 12-565-110N, Thermo Fisher Scientific Inc., Waltham, MA). During the experiments, the chambers are sealed to prevent evaporation-induced convection. Each motor is tracked for between 100-10,000 frames, and between 20 and 80 different motors are tracked at each concentration. The motors swim only in x-y plane because they settle near the surface and are only tracked when they are far from the sides of the glass well. The positions of the sphere centers are calculated in MATLAB from the intensity weighted centers of the spheres in each frame. Particle centers at each time are paired using an optical flow algorithm. Individual particle squared displacements are oversampled before they are averaged into a single mean square displacement. The time averaged velocity and the motor orientation are calculated from the sphere trajectory. The rotational velocity of the motors is calculated from the time averaged displacement of the motors orientation.

We compare the experiments with Brownian dynamics (BD) simulations of spherical circle swimmers in uniform fuel concentration. The simulations are carried out with the modified Langevin equations for 2-D shown in Equations 2-4 and assume that the standard 2-D Langevin equations are modified such that the displacement of the motors is the sum of its advective and Brownian components [10,33]. The advective velocity of the motors is only in the direction of orientation of the motors and the orientation is governed by a sum of the Brownian and time-averaged rotational velocity. The translational and rotational velocities used in the simulations are from linear fits of the experimental data and the Brownian diffusivities are set to match their theoretical values.

IV. RESULTS AND DISCUSSION

We previously reported that spherical bimetallic motors swim in H$_2$O$_2$ in the same manner as bimetallic nanorods [30]. In addition to the translational velocities typical of

bimetallic nanomotors, the spherical motors are also observed to possess a rotational velocity. Figure 1 shows representative traces of the 3 μm bimetallic nanomotors at H_2O_2 concentrations of 0.063%, 0.135%, 0.253%, 0.391%, 0.5%, 0.75%, 1.0%, and 1.25% (vol). Each trajectory shows the particle motion for 75 s. These plots show that the motors swim in circular patterns with an advective velocity that increases with the peroxide concentration. The orientation of a motors circular pattern is consistent in time, i.e. a motor that has a clockwise rotational velocity will always trace a clockwise circular pattern. As we increase concentration (from a to h) we see that the length of the path increases, denoting an increase in translational velocity, and the radius of curvature of the trajectory decreases, denoting an increase in rotational velocity. The motor translational swimming velocities are shown in Figure 2a as a function of the H_2O_2 concentration along with a linear fit of the translational velocity. The translational velocity increases linearly with concentration, which is consistent with previously published data for bimetallic nanomotors in hydrogen peroxide [6,26,27,30,39]. The motor angular velocities are shown in Figure 2b as a function of the H_2O_2 concentration along with a linear fit of the angular velocity. The rotational velocity varies linearly with concentration, which is what we would expect if the rotational component was a result of the asymmetric drag profile of the surface of the sphere. As seen in Figure 2 of Wheat et al. 2010 the fabrication method results in uneven distribution of mass on the surface of the motors and the extra mass on one side of the sphere results in an asymmetric drag profile of the sphere. The swimming motor would experience a slight spin towards the region of higher drag (the area with extra mass) and the magnitude of the spin would scale linearly with the translational velocity since the drag force scales with linearly with translational velocity at low Reynolds number [35]. In Figure 2 each error bar represents a single standard deviation. The large standard deviation for both the translational and rotational velocities is high due to the variability between motors.

While the translational velocity and rotational velocity describe the motion of the motor at any instant, the effective diffusivity can be used to describe the time averaged behavior. In Figure 3 we show the SDs of three individual motors at H_2O_2 concentrations of 0.135%, 0.253%, and 0.5%. The circle swimmers' SDs exhibit different behavior in short and long time scales [10,33,34]. For $t<\pi/\omega$ the SD increases from zero to a local maximum of approximately v^2/ω^2. At long times, $t>\pi/\omega$, the amplitude of the SD exhibits damped oscillations with a frequency that is roughly $\omega/2\pi$. The oscillations at long times are due to the motors swimming in a circular pattern as the center of the circle drifts away from the origin. The oscillations are damped because the displacement due to advection from the origin becomes large compared to the swimming radius. Each SD in Figure 3 has a different initial local maximum value and occurs at a different time. When the SD is scaled by v^2/ω^2 and time is scaled by π/ω the SD for each concentration will collapse onto a single line for $t<\pi/\omega$ before diverging to their long-time behavior (shown in Figure SM4). We can only draw qualitative insights from the SD due to the variability between different motors and the variability of a single motor over a period of time. In order to determine the time averaged motion of these motors as a function of time we can examine the MSD of the ensemble of particles as a function of H_2O_2 concentration.

The MSDs are shown in Figures 4a and 4b at H_2O_2 concentrations of 0.063%, 0.135%, 0.253%, 0.5%, 0.75%, 1.0%, and 1.25%. Each MSD represents an average of between 20 and 80 SDs at each concentration. Figure 4a shows the short-time region, $t<\pi/\omega$, of the MSD and Figure 4b shows the MSD at each concentration for approximately 150 s capturing both the short-time and long-time regions. In the short-time region shown in Figure 4a, the MSD increases as the swimmers complete half a rotation, consistent with the first phase of a sinusoid. The slope of the linear portion of the short-time region is given by Equation 7 and, as we predict, the slope increases with concentration. The short-time behavior of a circle swimmer is driven by the translational velocity of the swimmer and dampened by the rotational velocity. The long-time behavior of a circle swimmer is shown in Figure 4b. The slope of the long-time region in Figure 4b is described by Equation 6 and has a smaller slope than the short-time region because at long times both the rotational velocity and rotational diffusivity serve to limit net displacement from the origin. The distinct split between short and long time behavior is not observed at lower fuel concentrations because $\omega \sim D_r$ (for a 3 μm sphere in water $D_r=0.048$ rad^2/s). The experimental MSDs can be compared to theory (using Equation 5 or the BD simulations with the mean experimental velocities). We find that the shape of the MSDs qualitatively agree with Equation 5 in that they both exhibit a short-time behavior that transitions into a long-time region with a lower slope. The magnitude of the MSD slope at short-times (the short time diffusivity) agrees well with Equation 7 as is shown in Figure 5. At longer times, the experimentally measured slope is higher than predicted. The reason for the larger long-time slopes is discussed in detail during the presentation of Figure 6.

The largest discrepancy between the Equation 5 and the measured MSD is the MSD magnitude and the time at which the transition between the short and long time behaviors. The theory predicts that this transitions should occur at $t=\pi/\omega$, and have a magnitude of v^2/ω^2, where v and ω are the mean translational and rotational velocities from the average over all of the different motors at a given concentration. The theory and experiments differ in the transition stage of the MSD because the theory assumes all spheres have the mean translational and rotational velocities reported. In the experiments, motors, at any given concentration, exhibit large variations in the ratio of translational to rotational velocity (as revealed large error bars in Figure 2). These variations in individually measured translational and rotational velocities combined with the relatively small sample size (20-80 separate motors at any given concentration) leads to the discrepancy in height and location of the transition.

From the MSDs shown in Figure 4, we can quantify the short, D_S, and long time, D_L, diffusivities for circle swimmers. In Figure 5 the experimental D_S is plotted along with steady Brownian dynamics simulations with exact experimental velocities, steady Brownian dynamics simulations with velocities determined from linear fits of experimental values, Brownian dynamics simulations with amplified Brownian rotational diffusivities and velocities determined from linear fits of experimental values, and Equation 7 evaluated using fits of the experimentally measured translational and rotational motor velocities. The BD simulations with amplified

Brownian rotational diffusivities are BD simulations where the effective rotational diffusivities are increased to $4.5D_r$. All of the plotted diffusivities are scaled by the theoretical Brownian diffusivity of a 3μm sphere in water (D_o=0.145 μm^2/s).

Figures 5a and 5b show plots of the short-time normalized effective diffusivity as a function of the controlling parameter $v^2/2\omega$ and the H_2O_2 concentration. Figure 5a shows that the short-time effective diffusivity increases linearly with a slope and intercept of unity with the controlling relationship given in Equation 7. In Figure 5a all of the simulations and the experiments agree very well together. The experimental data does show some variation from the theory due to uncertainty in the translational and rotational velocities as well as uncertainty in D_S (due to the relatively small sample size of 20-80 motors at each concentration). From Figure 5a we also see that the theory presented in Equation 7 tends to slightly over-predict the short-time diffusivity because Equation 7 assumes that the effect of the rotational diffusivity is negligible over short-times when the rotational diffusivity actually serves to slightly limit D_S.

Figure 5b shows that the short-time effective diffusivity also varies linearly with concentration as predicted by Equation 9a since both v and ω vary linearly with H_2O_2 concentration. D_S measured in the experiments and BD simulations with exact experimental velocities fluctuate about the theoretical solution, while the BD simulations with fits of the velocities agree well with the theory. Figure 5a suggests that the D_S of the experiments and the BD simulations with exact experimental velocities fluctuate about the theoretical solution in Figure 5b due to the deviation of experimental velocity values from the linear dependence. The swimming motion of the motors results in short-time diffusivities that are between two hundred and one thousand times greater than the Brownian diffusivity. However, due to the circle swimming behavior of motors, the short-time diffusivity is smaller than the long-time diffusivity of a rotationally diffusive swimmer like a bimetallic nanorod or a platinum coated Janus particle in H_2O_2 with the same velocity.

Figures 6a and 6b respectively show the long-time diffusivity scaled by D_o as a function of $v^2/[2D_r(1+(\omega/D_r)^2)]$ (from Equation 6) and the fuel concentration for the experimental data, Brownian dynamics simulations with exact experimental velocities, Brownian dynamics simulations with velocities determined from linear fits of experimental values, Brownian dynamics simulations with amplified Brownian rotational diffusivities and velocities determined from linear fits of experimental values, and the theoretical long-time diffusivity given by Equation 6. In Figure 6a the D_L from Equation 6 shows up as a line with a slope and a y-intercept of unity. The D_L from all of the BD simulations follow the theory, while the experimental D_L shows some scatter. The deviations of the experimentally determined D_L originate from the uncertainty of the translational and rotational velocities. A sensitivity analysis of Equation 6 shows that an uncertainty in the measurement of the translational and rotational velocities of 10% can account for this deviation. It is important to note that in order to collapse all on the diffusivities onto the theory that the appropriate rotational diffusivities of the systems, i.e. for the

experiments and for the unsteady BD simulations a rotational diffusivity of $4.5D_r$ was used. Another source for the deviation is the fact that D_L is determined from a heterogeneous population of motors each with their own v and ω that are aggregated into a single D_L value.

In Figure 6b the theoretical solution given by Equation 6 and the steady BD simulations with velocities determined from linear fits of experimental values are in good agreement and suggest that D_L should increase at low concentration before they asymptote to a D_L of roughly a third of the measured D_L at high H_2O_2 concentrations. The measured D_L increases from 0.063% to a local maximum at 0.135% H_2O_2 concentration and then decreases and is relatively constant at high H_2O_2 concentrations, where ω is large compared to D_r. At high H_2O_2 concentrations, $\omega/D_r > 10$, D_L is approximately 100 times higher than D_o but only an eighth of the short-time diffusivity because the long-time diffusivity scales roughly as $v^2/(1+\omega^2)$ instead of v^2/ω. The measured D_L dips at a H_2O_2 concentration of 1.25% due to the trends of the velocities shown in Figure 2, the variability of the motors over a relatively small sample size (47 individual motors at 1.25% compared to thousands for the simulations), and a selection bias in the experimental data. The rotational velocity is 27% higher than expected at a H_2O_2 concentration of 1.25% based on the trend of the rotational velocity at the first six concentrations without a corresponding higher than expected translational velocity. From Equation 6 we can see that this results in a D_L that is 50% lower than expected. The MSD is made up of the average of a group of motors SDs. The shape of the individual SDs is determined by its rotational and translational velocity pair. At 1.25% there is a higher percentage of motors with higher rotational velocities and lower translational velocities (compared to the mean values) than at the other concentrations (look at Figure SM 5 for individual SDs at 0.5% and 1.25%). This issue is in part due to the relatively small sample size of our data and a small selection bias that is most prevalent at this concentration. The selection bias is due to the fact that motors with a high rotational velocity and low translational velocity tend to stay in the field of view of the microscope (and thus be tracked longer) than motors with high translational velocities and low rotational velocities. This bias becomes more prevalent when the motors, on average, have a high translational velocity. The steady BD simulations with exact experimental values predict a trend similar to that of the experimental data, except that the D_L asymptotes to a value that is roughly a third of the experimentally measured D_L at high H_2O_2 concentrations. The fact that the steady BD simulations and theory all agree on the asymptotic value of D_L at high H_2O_2 concentrations, but the experimental D_L is three times higher suggests that there is an underlying physical mechanism influencing the experiments that is not captured by the steady BD simulations or Equation 6.

In order to understand the discrepancy between the measured and theoretical predictions of the long-time diffusivity in Figure 6b it is useful to examine what parameters contribute to the shape of the MSD [36]. For a perfect circle swimmer, i.e. a particle with constant translational and rotational velocity (no Brownian motion or other perturbations to particle motion or orientations), the average slope of the long-time region would be zero and the MSD would be a

perfect sinusoid. If the circle swimmer were to experience Brownian translational motion but not Brownian rotational motion, i.e. the angular velocity is constant, then the average slope of the long-time region would be the Brownian translational diffusivity D_o. This holds regardless of the translational and rotational velocity supplied by the motors. If the circle swimmer experiences Brownian rotational and translational motion then the slope of the diffusive region is given by Equation 6. For the range of experimental translational and rotational velocities in this paper the addition of rotational Brownian motion results in long-time diffusivities between 50 and 150 times greater than D_o. The reason why the long-time diffusivity that we measure increases one to two orders of magnitude upon the addition of randomness to the orientation of the motors, in this case due to Brownian motion, is because the unsteadiness of the orientation allows for the translational and rotational velocities to take the motor further, on average, from its origin. Therefore, we see that the long-time diffusivity of circle swimmers is strongly modulated by the unsteady orientation of the motors.

We believe that the measured long-time effective diffusivity is greater than the BD simulations and analytical predictions because the unsteadiness of the motors orientation is greater than predicted by the theoretical Brownian rotational diffusivity. This is significant because it illustrates that motors fabricated with unsteady swimming mechanisms will have higher long-time diffusivities than steady motors. For circle swimmers the experimental rotational diffusivity can be calculated from a quadratic fit of the experimental mean squared angular displacement [10]. We observe a weak linear dependence of the measured rotational diffusivity with concentration with a maximum measured rotational diffusivity of six times what is expected due to Brownian motion at a H_2O_2 concentration of 1.25%. We hypothesize that the increased long-time diffusivity measured in the experiments, as compared to the Brownian dynamics simulations and Equation 6, is due to some additional unsteadiness in the orientation of the motor above what is expected due to Brownian rotational motion. This unsteadiness is potentially driven by fluctuations in the RICA force experienced by the motors. The fluctuations may be due to non-uniform adsorption of anions or other species, intermittent occurrences of the O_2 reduction reactions, or inhomogeneity of H_2O_2 concentration. Regardless of their source, any perturbation to the RICA force (especially the rotational component) causes an increase in the long-time diffusivity. The unsteady perturbations of the RICA mechanism enhance the effective diffusivity in the same way that Brownian rotational diffusivity increases the long-time diffusivity of a perfect circle swimmer. The validity of this assertion can be seen in Figure 6a where we have collapsed the experimental long-time diffusivities around the theory by using an amplified rotational diffusivity. In Figure 6b we include the results of the unsteady simulations (the velocities are based on linear fits of the experimental data) to show that effectively increasing the rotational Brownian diffusivity causes an increase in the motors long-time diffusivity. We make the motor motion unsteady by increasing the magnitude of the Brownian rotational diffusivity to $4.5D_r$ based on our findings from the mean squared angular displacement and from Figure 6a. If the average fluctuation magnitude is held constant with H_2O_2

concentration we observe reasonable agreement of the long-time unsteady BD simulations diffusivity to the experimentally measured long-time diffusivity at high H_2O_2 concentrations.

Figure 6b shows a local maximum as a function of the concentration in the long-time effective diffusivity for the experiments as well as the BD simulations with exact experimental velocities. This maximum is not predicted from Equation 9b nor observed in the BD simulations with linear fits of the experimental velocities. The observed maximums that occur around peroxide concentrations of 0.135% in Figure 6 are due to a high translational velocity and small angular velocity compared to linear behavior of the translational and rotational velocities at those concentrations. The translational and angular velocities deviate from the linear trend as shown in Figure 2. The deviations are not systematic (i.e. not because the velocity as a function of concentration exhibit some significant nonlinearity). The deviation from the fit is due to natural variation of the swimmer's velocity. We expect that with a larger sample volume or more uniform motors, we may not observe the asystematic variation in velocity that yields the maximum in effective diffusivity. We examine the conditions under which we expect to observe maximums in the long-time effective diffusivity in the next section.

V. MAXIMUM OF EFFECTIVE DIFFUSIVITY

The maximum in effective diffusivity observed in the experiments and simulations is a result of asystematic variations in the translational and angular velocity, but we provide some discussion of the conditions under which we might expect to observe a local maximum in effective diffusivity due to systematic velocity dependence on a physical controlling parameter, in this case concentration.

It is instructive to consider a general case, Equation 8, for the dependence of the velocity on a physical controlling parameter, such as concentration, since non-linear dependencies have been measured [9,28,38-40] and predicted [9,26,27,28] for a variety of motor propulsion mechanisms. Figure 7a shows the contour map of the normalized long-time effective diffusivity calculated from Equation 6 as a function of H_2O_2 concentration, and order of power dependence of the rotational velocity on H_2O_2 concentration, b, where the motor's translational and angular velocities can have a nonlinear dependence on the fuel concentration ($v \propto C^a$ and $\omega \propto C^b$ respectively). In Figure 7a, the translational velocity is held linearly dependent on H_2O_2 concentration, $a=1$, for all values of b. As is predicted by the scaling in Equation 9b, when $b \leq a$ Figure 7a shows that D_L increases monotonically and asymptotes at high H_2O_2 concentrations. When $b>a$ D_L increases with concentration to a maximum and decays to an asymptote at high H_2O_2 concentrations. The magnitude of the peak diffusivity increases as the non-linearity of the rotational velocity, b, increases. The maximum occurs when ω increases at a faster rate than v and the rotational velocity dampens the long-time diffusivity at high translational velocities.

Another mechanism by which a maximum in D_L could be achieved is by modulation of the rotational diffusivity. Figure 7b shows the long-time diffusivity as calculated from Equation 6, plotted against the rotational diffusivity scaled by the mean rotational velocity.

Modulation of rotational diffusivity has been shown in this work (Figure 6a) and by Takagi et al. 2013 [31]. A maximum in D_L is predicted by Equation 6 when the rotational diffusivity equals the rotational velocity. This suggests that there is an optimal amount of randomness in a circle swimmers motion that can maximize its effective diffusivity. Just enough randomness in the orientation allows the motor to break its' circular trajectory, while too much makes it so that the motor is not able to advect away before reorienting and traveling in a different direction.

VI. SUMMARY

Spherical catalytic bimetallic micromotors fabricated as described in Wheat et al. 2010 [30] have both translational and rotational velocity that vary with H_2O_2 concentration. The rotational velocity is likely due to asymmetry of the drag profile of the sphere caused by uneven metal coatings in the motor fabrication steps. We show that generic circle swimmer motors (not necessarily catalytic motors) exhibit short and long-time diffusivities that scale as $v^2/2\omega$ and $v^2/[2D_r(1+(\omega/D_r)^2)]$ respectively. The short-time diffusivity is larger than the long-time diffusivity because the long-time diffusivity is proportional to $v^2/(1+\omega^2)$ instead of v^2/ω. $D_S > D_L$ suggests that although a circle swimming motor has a reduced diffusivity at long-times compared to a rotationally diffusive swimmer it samples a much larger region of the space over which it diffuses. The motors transition from short-time to long-time behavior at a time of $\pi/\omega(C)$. Therefore, the governing diffusive time scale varies as a function of hydrogen peroxide concentration. This means that when observed over short-times, or when the motors are confined to small spaces, the motors will appear to have a different diffusivity than at long-times or in large spaces. This effect could result in interesting behavior when a large number of these motors are placed in close proximity because their swimming pattern would lead to a high collision probability.

We also show that artificial swimmers can exhibit maxima in long-time effective diffusivities if the motors have nonlinear translational or rotational velocities, or if the rotational diffusivity is a function the physical controlling parameter, in this work fuel concentration. Here, we do not observe significant nonlinear dependencies of v or ω, and owe the measured maximum in long-time diffusivity to measured translational and rotational velocities that deviate from the expected linear trend at low H_2O_2 concentrations. The combination of diffusive time scales and non-monotonic diffusivity of circle swimming catalytic motors as a function of fuel concentration suggests that we can expect complex particle responses in confined geometries and in spatially dependent fuel concentration gradients.
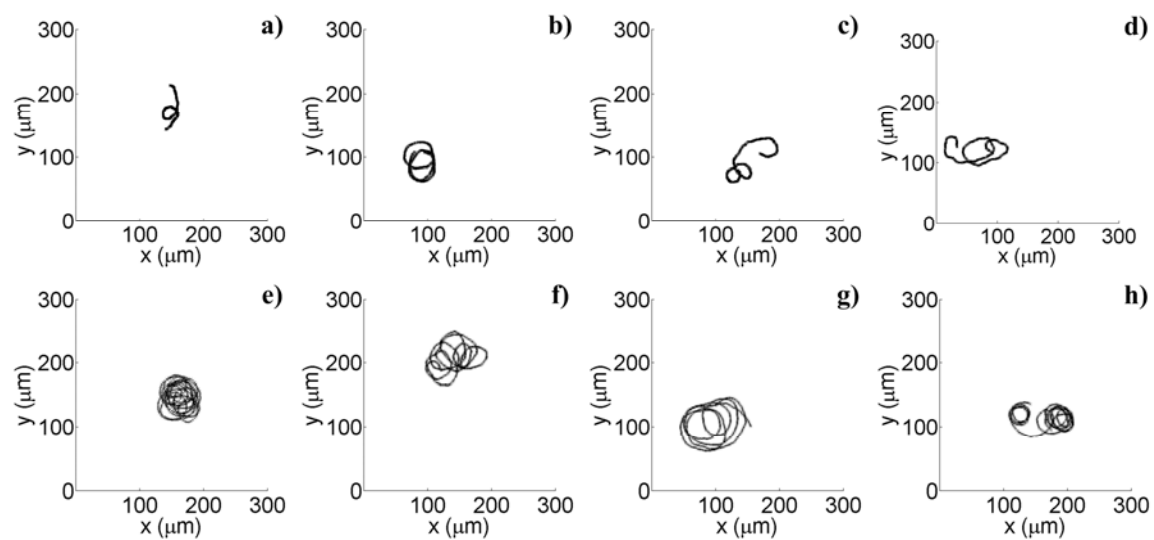
Figures


Figure 1. Representative traces of the 3 μm spherical bimetallic motors path over 75 s at each concentration. The hydrogen peroxide concentration increases from a) to h) [0.063 0.135 0.253 0.391 0.5 0.75 1.0 1.25] (volume %).
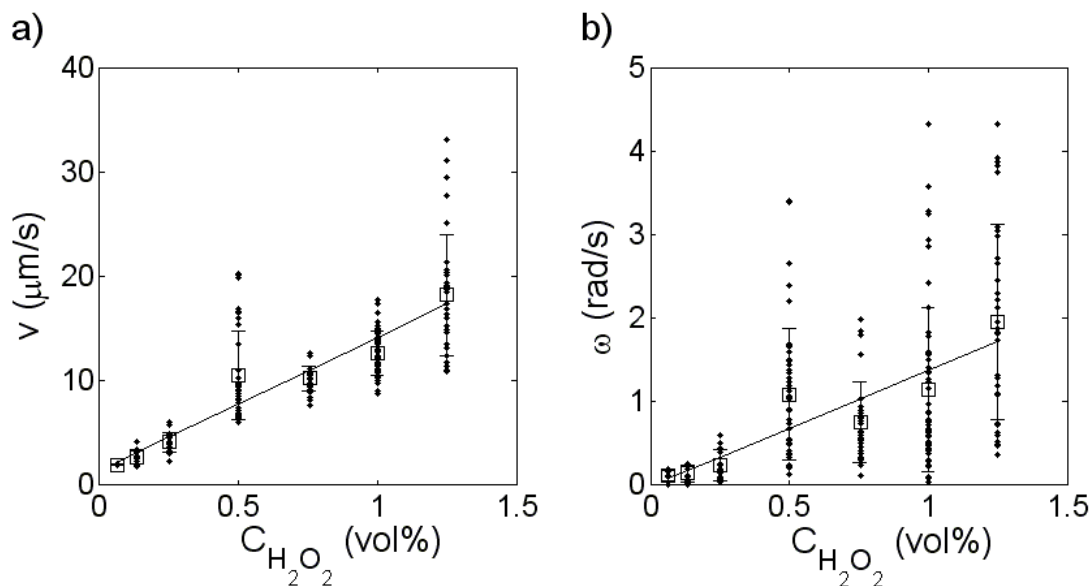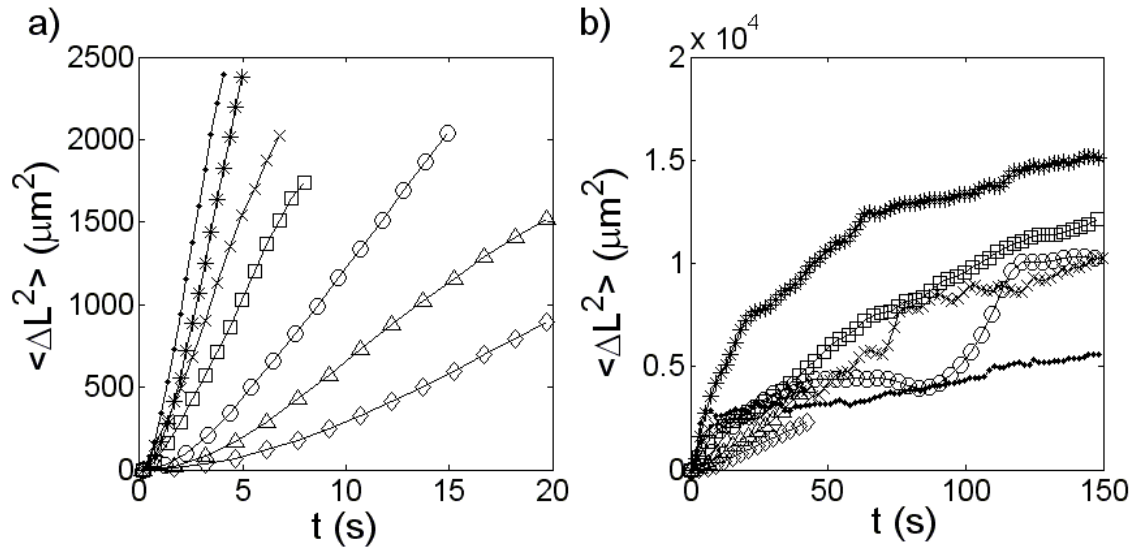
Figure 2. a) Average bimetallic spherical micromotor velocity versus hydrogen peroxide concentration. The error bars represent one standard deviation of the ensemble of time averaged velocities. **b)** Average bimetallic spherical micromotor rotational velocity versus hydrogen peroxide concentration. Each individual motor velocity ($\bullet$) is plotted along with, the mean value ($\square$), and a linear fit of the velocity. The error bars represent one standard deviation of the ensemble of time averaged velocities.
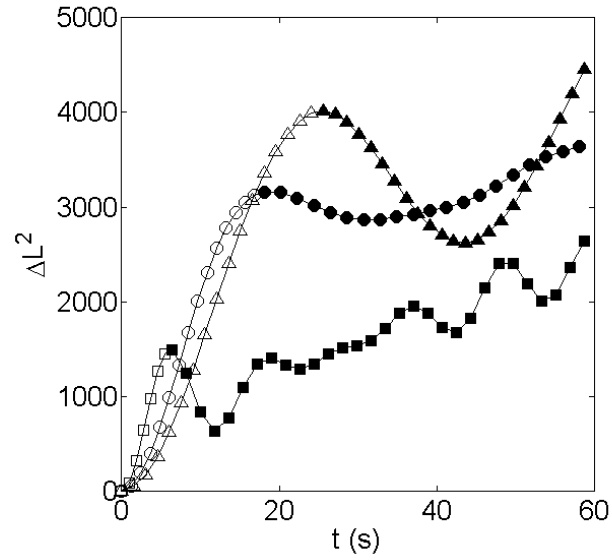
Figure 3. Squared displacement of individual bimetallic spherical micromotors versus time for hydrogen peroxide concentrations of 0.135% (Δ),0.253% (○), and 0.5% (□). For each concentration there is a short time (open symbols) and a long time (filled symbols) diffusivity region. The short time region is marked by the sharp increase of the SD and corresponds to the motor completing half of a rotation. The second region is marked by dampened oscillations that correspond to displacement of the circular motor trajectories.

Figure 4. **a)** MSD of bimetallic spherical micromotors versus time for all concentrations of hydrogen peroxide at short times ($t < \pi/\omega$). **b)** MSD versus time at all times. The hydrogen peroxide concentrations shown are: 0.063% (◊), 0.135% (Δ), 0.253% (○), 0.5% (□), 0.756% (x), 1.0% (*), and 1.25% (●). The slope of the MSD gives the effective diffusivity. The slope of the MSD at short times ($t < \pi/\omega$) is the short-time effective diffusivity. The slope of the MSD at long times ($t > \pi/\omega$) is the long-time effective diffusivity.
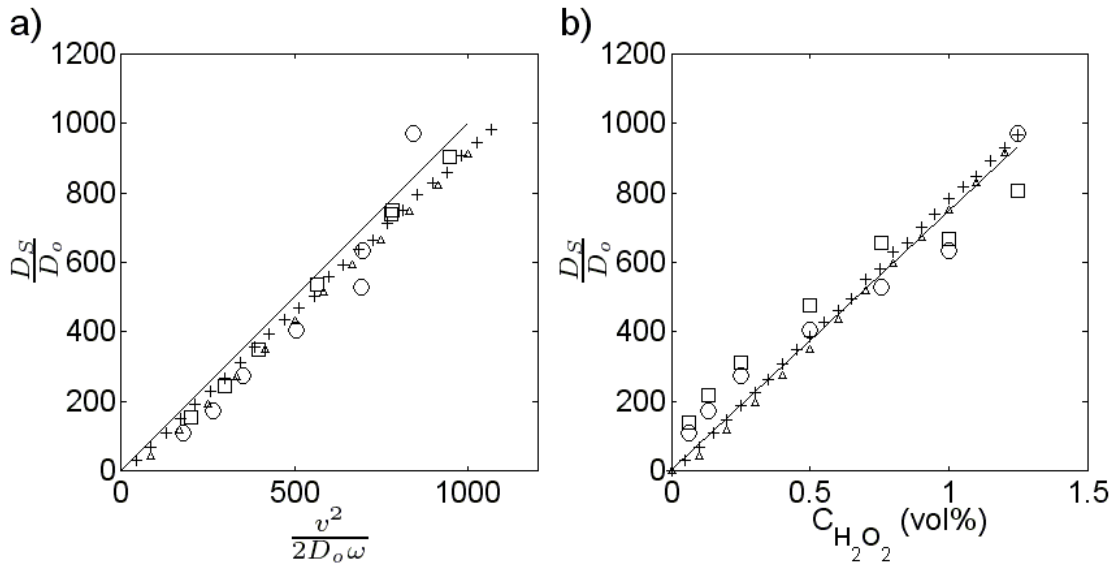
Figure 5. a) Short-time effective diffusivity of bimetallic spherical micromotors scaled by Brownian diffusivity versus the controlling parameter, $v^2/2\omega$, scaled by the Brownian diffusivity. **b)** Short-time effective diffusivity of bimetallic spherical micromotors scaled by the Brownian diffusivity versus hydrogen peroxide concentration. The experimental data ($\circ$) is plotted along with steady Brownian dynamics simulations with exact experimental velocities($\square$), steady Brownian dynamics simulations with velocities determined from fits of experimental values($\bullet$), unsteady Brownian dynamics simulations with velocities determined from fits of experimental values (Δ), and the fit of Equation 7 (solid line). The short time effective diffusivity is the slope of the MSD at times less than π/ω shown in Figure 4a.
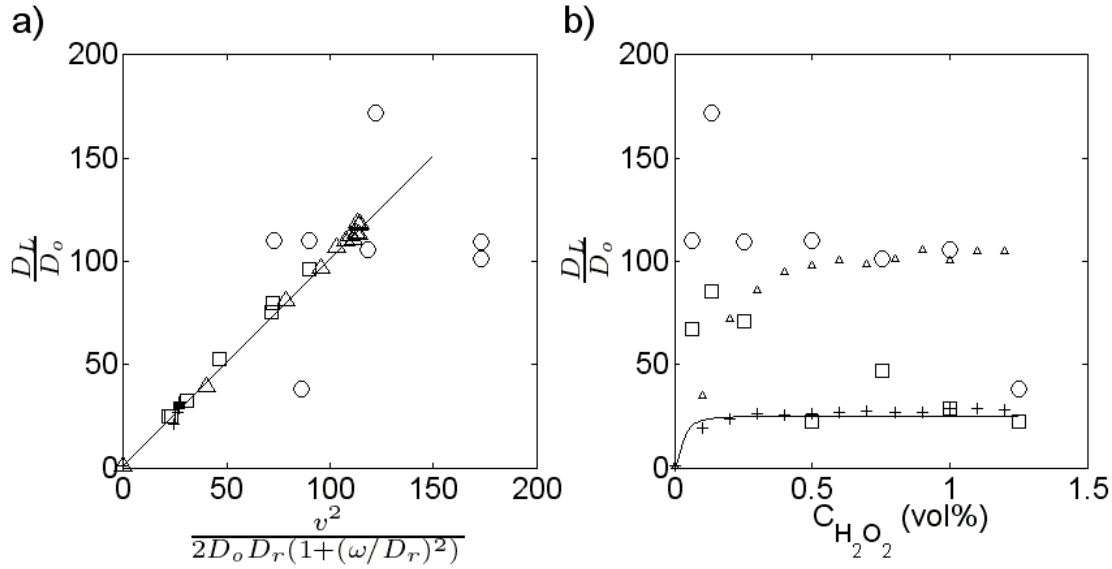
Figure 6. a) Long-time effective diffusivity of bimetallic spherical micromotors scaled by the Brownian diffusivity versus the controlling parameter, $v^2/[2D_r(1+(\omega/D_r)^2)]$, scaled by the Brownian diffusivity. **b)** Long-time effective diffusivity of bimetallic spherical micromotors scaled by the Brownian diffusivity versus hydrogen peroxide concentration. The experimental data ($\circ$) is plotted along with steady Brownian dynamics simulations with exact experimental velocities ($\square$), steady Brownian dynamics simulations with velocities determined from fits of experimental values($\bullet$), unsteady Brownian dynamics simulations with velocities determined from fits of experimental values (Δ), and the scaling shown in Equation 6 (solid line). The long-time effective diffusivity is the slope of the MSD at times longer than π/ω shown in Figure 4b.
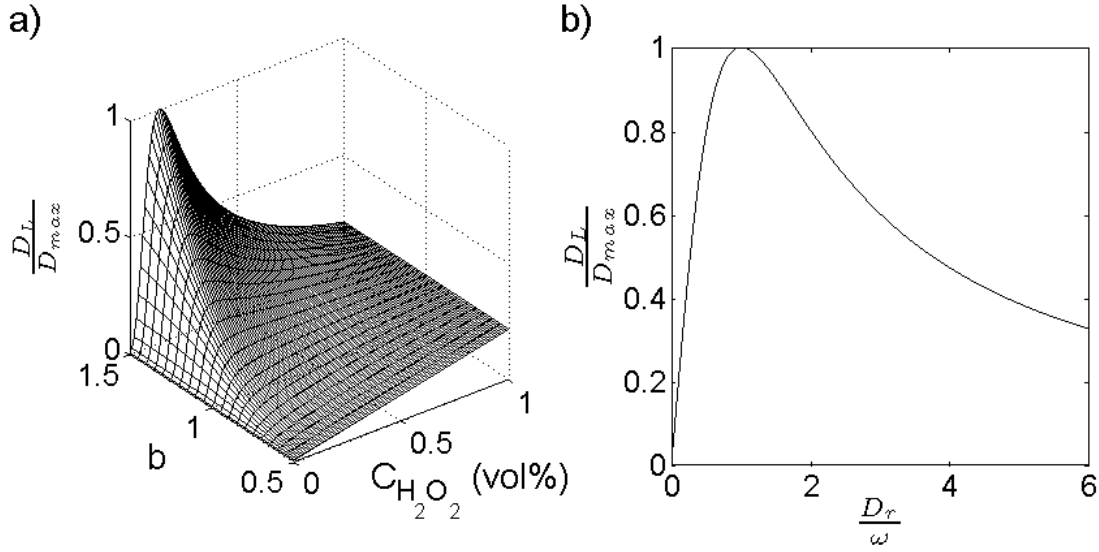
Figure 7. a) Space-field map of the normalized long-time effective diffusivity calculated from Equation 6 as a function of hydrogen peroxide concentration, and order of power dependence of the rotational velocity on concentration ($\omega=K_1C^b$). The long-time diffusivity is normalized by the maximum diffusivity within the sample space. The translational velocity is linearly dependent on concentration for all values of b. **b)** The long-time diffusivity calculated from Equation 6 vs. rotational diffusivity. The diffusivity is scaled by the maximum diffusivity within the sample space and the rotational diffusivity is scaled by the rotational velocity.

REFERENCES

[1]   M. G. L. van den Heuvel and C. Dekker, Science **317**, 333–336 (2007).
[2]   A. Goel and V. Vogel, Nature Nanotechnology **3**, 465–475 (2008).
[3]   C. Brunner, C. Wahnes, and V. Vogel, Lab Chip **7**, 1263 (2007).
[4]   R. K. Doot, H. Hess, and V. Vogel, Soft Matter **3**, 349 (2007).
[5]   H. Hess, G. D. Bachand, and V. Vogel, Chemistry-a European Journal **10**, (2004).
[6]   W. F. Paxton, K. C. Kistler, C. C. Olmeda, A. Sen, S. K. St. Angelo, Y. Cao, T. E. Mallouk, P. E. Lammert, and V. H. Crespi, J Am Chem Soc **126**, 13424–13431 (2004).
[7]   W. F. Paxton, A. Sen, and T. E. Mallouk, Chem. Eur. J. **11**, 6462–6470 (2005).
[8]   S. Fournier-Bidoz, A. C. Arsenault, I. Manners, and G. A. Ozin, Chem. Commun. 441 (2005).
[9]   J. R. Howse, R. A. L. Jones, A. J. Ryan, T. Gough, R. Vafabakhsh, and R. Golestanian, Phys. Rev. Lett. **99**, 048102 (2007).
[10] S. Ebbens, R. Jones, A. Ryan, R. Golestanian, and J. Howse, Physical Review E **82**, 0153304(R) (2010).
[11] N. Chaturvedi, Y. Hong, A. Sen, and D. Velegol, Langmuir 1692–1712 (2010).
[12] P. Dhar, T. M. Fischer, Y. Wang, T. E. Mallouk, W. F. Paxton, and A. Sen, Nano Letters **6**, 66–72 (2006).
[13] W. F. Paxton, P. T. Baker, T. R. Kline, Y. Wang, T. E. Mallouk, and A. Sen, J. Am. Chem. Soc. **128**, 14881–14888 (2006).
[14] Y. Wang, R. M. Hernandez, D. J. Bartlett Jr, J. M. Bingham, T. R. Kline, A. Sen, and T. E. Mallouk, Langmuir **22**, 10451–10456 (2006).
[15] K. M. Manesh, M. Cardona, R. Yuan, M. Clark, D. Kagan, S. Balasubramanian, and J. Wang, ACS Nano (2010).
[16] R. F. Ismagilov, A. Schwartz, N. Bowden, and G. M. Whitesides, Angewandte Chemie **114**, 674–676 (2002).
[17] S. J. Ebbens and J. R. Howse, Soft Matter **6**, 726–738 (2010).
[18] J. Wang, ACS Nano **3**, 4–9 (2009).
[19] J. Burdick, R. Laocharoensuk, P. M. Wheat, J. D. Posner, and J. Wang, J Am Chem Soc **130**, 8164–8165 (2008).
[20] S. Sundararajan, P. E. Lammert, A. W. Zudans, V. H. Crespi, and A. Sen, Nano Lett. **8**, 1271–1276 (2008).
[21] T. R. Kline, J. Iwata, P. E. Lammert, T. E. Mallouk, A. Sen, and D. Velegol, Journal of Physical Chemistry B-Condensed Phase **110**, 24513–24521 (2006).
[22] P. Calvo-Marzal, K. M. Manesh, D. Kagan, S. Balasubramanian, M. Cardona, G.-U. Flechsig, J. Posner, and J. Wang, Chem. Commun. (2009).
[23] M. Ibele, T. E. Mallouk, and A. Sen, Angewandte Chemie International Edition **48**, 3308–3312 (2009).
[24] Y. Hong, N. M. K. Blackman, N. D. Kopp, A. Sen, and D. Velegol, Phys. Rev. Lett. **99**, (2007).
[25] S. Balasubramanian, D. Kagan, K. M. Manesh, P. Calvo-Marzal, G.-U. Flechsig, and J. Wang, Small **9999**, NA (2009).
[26] J. L. Moran, P. M. Wheat, and J. D. Posner, Phys. Rev. E **81**, 065302 (2010).
[27] J. L. Moran and J. D. Posner, Journal of Fluid Mechanics **680**, 31–66 (2011).
[28] J. G. Gibbs and Y.-P. Zhao, Small **5**, 2304–2308 (2009).
[29] J. G. Gibbs, S. Kothari, D. Saintillan, and Y.-P. Zhao, Nano Lett. **11**, 2543–2550 (2011).

[30] P. M. Wheat, N. A. Marine, J. L. Moran, and J. D. Posner, Langmuir **26**, 13052–13055 (2010).

[31] D. Takagi, A.B. Braunshweig, J. Zhang, and M. J. Shelley, Phys. Rev. Lett. **110**, 038301 (2013).

[32] T. Mirkovic, N. S. Zacharia, G. D. Scholes, and G. A. Ozin, Small **6**, 159–167 (2010).

[33] S. van Teeffelen and H. Löwen, Phys. Rev. E **78**, 020101 (R) (2008).

[34] S. van Teeffelen, U. Zimmermann, and H. Löwen, Soft Matter **5**, 4510 (2009).

[35] J. Happel and H. Brenner, *Low Reynolds Number Hydrodynamics: With Special Applications to Particulate Media* (Springer, 1983).

[36] See Supplemental Material at [URL will be inserted by publisher] for MSD of circle swimmers with no Brownian motion, with Brownian translational motion but not Brownian rotational motion, and with both Brownian translational motion and Brownian rotational motion.

[37] J. G. Gibbs and Y.-P. Zhao, Appl. Phys. Lett. **94**, 163104–3 (2009).

[38] D. Kagan, P. Calvo-Marzal, S. Balasubramanian, S. Sattayasamitsathit, K. M. Manesh, G.-U. Flechsig, and J. Wang, Journal of the American Chemical Society **131**, 12082 (2009).

[39] R. Laocharoensuk, J. Burdick, and J. Wang, ACS Nano **2**, 1069–1075 (2008).

[40] B. Sabass and U. Seifert, The Journal of Chemical Physics **136**, 214507 (2012).